Spectroscopic Evidence for the Symmetric Location of Tyrosines D and Z in Photosystem II†

Dionysios Koulougliotis,‡ Xiao-Song Tang,§ Bruce A. Diner,§ and Gary W. Brudvig*,‡

Department of Chemistry, Yale University, 225 Prospect Street, New Haven, Connecticut 06511, and Central Research and Development Department, E. I. du Pont de Nemours & Company, Experimental Station, P.O. Box 80173, Wilmington, Delaware 19880-0173

Received September 21, 1994; Revised Manuscript Received December 19, 1994⊗

ABSTRACT: Saturation−recovery EPR spectroscopy has been used to probe the location of the redox-active tyrosines, Y_D (tyrosine 160 of the D2 polypeptide, cyanobacterial numbering) and Y_Z (tyrosine 161 of the D1 polypeptide), relative to the non-heme Fe(II) in Mn-depleted photosystem II (PSII). Measurements have been made on PSII membranes isolated from spinach and on PSII core complexes purified from the cyanobacterium *Synechocystis* sp. PCC 6803. In the case of *Synechocystis* PSII, site-directed mutagenesis of the Y_D residue to either phenylalanine (Y160F) or methionine (Y160M) was done to eliminate the dark-stable $Y_D^{\bullet}$ species and, thereby, allow direct spectroscopic observation of the $Y_Z^{\bullet}$ EPR signal. The spin−lattice relaxation transients of both $Y_D^{\bullet}$ and $Y_Z^{\bullet}$ were non-single-exponential due to a dipolar interaction with one of the other paramagnetic species in PSII. Measurements on CN^--treated, Mn-depleted cyanobacterial PSII, in which the non-heme Fe(II) was converted into its low-spin, diamagnetic state, proved that the non-heme Fe(II) was the sole spin−lattice relaxation enhancer for both the $Y_D^{\bullet}$ and $Y_Z^{\bullet}$ radicals. This justified the use of a dipolar model in order to fit the saturation−recovery EPR data, which were taken over the temperature range 4−70 K. The dipolar rate constants extracted from the fits were identical in magnitude and had the same temperature dependence for both $Y_D^{\bullet}$ and $Y_Z^{\bullet}$. The observation of identical dipolar interactions between $Y_D^{\bullet}$ and $Y_Z^{\bullet}$ and the non-heme Fe(II) shows that the distance from each tyrosine to the non-heme Fe(II) is the same. The calculated distance of 37 ± 5 Å between Y_D or Y_Z and the non-heme Fe(II) agrees well with the distance predicted from the structure of the reaction center from purple bacteria. These results constitute the first spectroscopic evidence for a symmetric location of tyrosines D and Z in PSII and are consistent with the existence of a C_2 symmetry axis among the chromophores of PSII, as in the purple bacterial reaction center.

Photosystem II (PSII) is a multisubunit integral membrane protein complex used by higher plants and cyanobacteria to catalyze water oxidation and plastoquinone reduction. Although its multiple redox-active components have been the object of detailed biophysical characterization during the last few decades, their three-dimensional arrangement is still elusive. The X-ray crystal structures of the photosynthetic reaction centers from the purple non-sulfur bacteria *Rhodopseudomonas viridis* (Deisenhofer et al., 1985) and *Rhodobacter sphaeroides* (Chang et al., 1986; Allen et al., 1988), together with significant similarities in the primary structures of the L and M subunits of the bacterial reaction center and the D1 and D2 subunits of PSII, respectively, have provided some insight into the structure of the D1/D2 complex. For example, this structural analogy made possible the assignment of specific functional amino acids in PSII (Michel et al., 1986; Trebst, 1986; Michel & Deisenhofer, 1988), as well as a prediction of the folding pattern of the five transmembrane helices proposed to constitute each of the D1 and D2 proteins (Michel et al., 1986; Trebst, 1986). Subsequently, immunological studies provided experimental evidence for the predicted topology of the membrane-spanning helices of the D1 protein (Sayre et al., 1986).

By using the available crystal structures of the bacterial reaction centers as a framework, computer modeling has been used to produce three-dimensional models of the D1 and D2 proteins. Two models have been constructed in order to investigate the Q_B/herbicide-binding site on the electron-acceptor side of the PSII reaction center (Bowyer et al., 1990; Tietjen et al., 1991). Models of the structure of electron-donor side components in PSII have also been generated (Svensson et al., 1990; Ruffle et al., 1992). While in purple photosynthetic bacteria a cytochrome acts as the reducing agent of the oxidized primary electron donor, in PSII this function is much more complex. At least three distinct electron-donation pathways exist to the oxidized primary electron donor in PSII, P_{680}^+. These pathways (Buser et al., 1990) lead to the oxidation of a tyrosine residue known as Y_D, of cytochrome b_{559} via a redox-active chlorophyll known as Chl_Z (Thompson & Brudvig, 1988), and of the tetranuclear Mn complex via a second redox-active tyrosine residue known as Y_Z (Hoganson & Babcock, 1988). On the basis of the predicted folding model of the D1/D2 complex, iodide labeling experiments indicating that tyrosine residues are involved in electron donation to the PSII reaction center (Takahashi et al., 1986; Ikeuchi & Inoue, 1987) and deuteration experiments identifying Y_D and Y_Z as tyrosine residues (Barry & Babcock, 1987, 1988; Boerner

† This work was supported by the National Institutes of Health (GM32715 and GM36442) (to G.W.B.) and by NRI/CRGP of the U.S. Department of Agriculture (to B.A.D.).

‡ Yale University.

§ E. I. du Pont de Nemours & Co.

⊗ Abstract published in *Advance ACS Abstracts,* February 15, 1995.

0006-2960/95/0434-2850$09.00/0

& Barry, 1993); site-directed mutagenesis experiments were carried out to identify the two redox-active tyrosine residues in PSII. These experiments definitively showed that Y_D is Tyr160 (Vermaas et al., 1988; Debus et al., 1988a) and Y_Z is Tyr161 (Debus et al., 1988b; Metz et al., 1989) in the D2 and D1 proteins, respectively.

The computer-generated models of the three-dimensional structure of the donor side PSII components (Svensson et al., 1990; Ruffle et al., 1992) predict the immediate environment of the two tyrosine radicals and also arrange them symmetrically around the primary electron donor, P_{680}. Thus, the pseudo-C_2-symmetry axis seen in the arrangements of the L/M polypeptides and of the chromophores in the bacterial reaction center is also predicted to be present in PSII. In addition, the dramatically different kinetics of oxidation of Y_D and Y_Z is well established (Hoganson & Babcock, 1988; Buser et al., 1990). This also echoes the well-documented fact of the inactivity of one of the C_2-symmetry-related branches of bacterial reaction centers in charge separation (Kirmaier & Holten, 1987).

In this work, we have used the pulsed EPR technique of saturation–recovery (Hyde, 1979) to probe the locations of Y_D and Y_Z relative to the non-heme Fe(II) in PSII. Past work has shown that the spin–lattice relaxation of $Y_D^\bullet$ is enhanced via dipolar interactions with other paramagnetic centers in PSII (Styring & Rutherford, 1988; Evelo et al., 1989; Beck et al., 1990; Hirsh et al., 1992; Hirsh & Brudvig, 1993). In Mn-depleted PSII, the non-heme Fe(II) was assigned as the relaxation enhancer of $Y_D^\bullet$ (Hirsh et al., 1992). By using cyanide to convert the non-heme Fe(II) to its low-spin diamagnetic form (Sanakis et al., 1994), we have confirmed that the non-heme Fe(II) is the sole relaxation enhancer of $Y_D^\bullet$ in Mn-depleted PSII. In order to prepare a sample in which to probe the dipolar interaction of the non-heme Fe(II) with $Y_Z^\bullet$, two different site-directed mutants of PSII in the cyanobacterium *Synechocystis* sp. PCC 6803 were constructed, in which the Y_D tyrosine residue (D2-Tyr160) was changed to either phenylalanine (Y160F) or methionine (Y160M). These mutants were isolated by Dexter Chisholm and will be described in a forthcoming publication (Tang et al., 1995). In PSII core preparations purified from these mutants, freezing under illumination results in the trapping of $Y_Z^\bullet$ without any contribution from the stable free radical, $Y_D^\bullet$, normally present in wild-type preparations. The independent study of the spin–lattice relaxation behavior of $Y_Z^\bullet$ is, thus, made possible. Analysis of the dipolar enhancement of the spin–lattice relaxation rate of both $Y_D^\bullet$ and $Y_Z^\bullet$ has allowed us to determine the locations of these tyrosines relative to the non-heme Fe(II). These results provide the first spectroscopic evidence for the symmetric location of tyrosines D and Z in PSII and are consistent with the existence of a C_2 symmetry axis among the chromophores of PSII.

MATERIALS AND METHODS

Sample Preparation. PSII membranes were isolated from market spinach leaves by a modified version (Beck et al., 1985) of the isolation procedure described by Berthold et al. (1981). NH_2OH treatment was used in order to deplete PSII of manganese (~5% residual Mn) according to the procedure described in Hirsh et al. (1992). The CN^- derivative of Mn-depleted PSII was prepared according to Sanakis et al. (1994) and also as described in Koulougliotis et al. (1994). A dark incubation time of 4–6 h was needed for complete conversion of the non-heme Fe(II) to its low-spin state (vide infra). Chemical reduction of the CN^--treated samples was performed by adding 50 mM sodium dithionite from a degassed stock solution prepared and adjusted to pH 8.0 just prior to use. The sample concentration for saturation–recovery EPR experiments was between 4 and 6 mg of Chl/mL. Induction of $Y_D^\bullet$ in Mn-depleted, CN^--treated samples was achieved by illumination (700 W/m^2) at 0 °C for 8 min, followed by dark adaptation for 3 min and freezing at 77 K in complete darkness. The $Y_D^\bullet$ EPR signal in Mn-depleted PSII was used as a spin standard for the spin quantitation of the Q_A^- free radical species (induced in Mn-depleted, CN^--treated, dithionite-reduced PSII) (Koulougliotis et al., 1994; Sanakis et al., 1994).

The PSII core complexes from *Synechocystis* sp. PCC 6803, depleted of the Mn cluster, were prepared by the procedure of Tang and Diner (1994), as modified by Tang et al. (1995). The modifications include breaking the cells in buffer A containing 50 mM HEPES–NaOH (pH 7.2) instead of MES–NaOH (pH 6.0) and following the DEAE-Toyopearl ion-exchange chromatography by a second column step on hydroxylapatite, according to Rögner et al. (1990). The PSII core complexes are completely inactive for oxygen evolution as isolated and contain no EPR-detectable Mn. The core complexes were washed and resuspended, using a Centricon 100 (Amicon), in 0.4 M sucrose, 100 mM Tricine–NaOH (pH 8.0), 15 mM NaCl, and 5 mM $MgCl_2$ to a final concentration of ~10 mg of Chl/mL. In order to form the cyanide derivative, the core complexes were then diluted 10-fold (to 1 mg of Chl/mL) in the preceding buffer containing 340 mM NaCN (pH adjusted to 8.0) and incubated for 30 min at 0 °C. $K_3Fe(CN)_6$ was added to give a final concentration of 0.3 mM, and the sample was placed in an EPR tube. $Y_Z^\bullet$ was trapped by freezing under illumination with white light provided by a 150 W lamp (Cuda Products Corp. Model I-150). Further details on the trapping and spectroscopic properties of $Y_Z^\bullet$ will be provided in a forthcoming paper (Tang et al., 1995).

As a test of the transformation of the non-heme Fe(II) from high ($S = 2$) to low ($S = 0$) spin, 10 μL of 500 mM dithionite was added to 95 μL of the CN^--treated core complex, and the sample was incubated for another 7–10 min at 0 °C and then frozen in an EPR tube in the dark. Measurement of the $g = 2.0045$ Q_A^- EPR signal showed that a 30-min incubation with cyanide was optimal for the spin transformation of the iron.

Instrumentation. Saturation–recovery EPR experiments and continuous-wave (cw) EPR spectroscopy were performed on a home-built X-band pulsed EPR spectrometer (Beck et al., 1991). The temperature was controlled with an Oxford ESR 900 liquid helium cryostat and calibrated by using a Si diode sensor at the sample position.

THEORY

Saturation–recovery EPR has already been used in our laboratory in order to probe the location of the $Y_D^\bullet$ radical in PSII (Hirsh et al., 1992; Hirsh & Brudvig, 1993). By following the theory of spin–lattice relaxation enhancement of a paramagnetic species due to dipole–dipole interactions with neighboring paramagnets (Bloembergen, 1949; Abrag-

am, 1955, 1961), a dipolar model was developed in order to explain the non-single-exponential spin−lattice relaxation kinetics of the $Y_D^{\bullet}$ radical in PSII (Hirsh et al., 1992). According to this model, if we can assume the existence of only pairwise interactions between slow- and fast-relaxing paramagnets, we can discern two major contributions to the spin−lattice relaxation rate of the observed (slow) spin: (i) an isotropic term, denoted $k_{1\text{scalar}}$, incorporating the intrinsic relaxation rate of the species (k_{1i}) and the relaxation arising from its exchange coupling (k_{1ex}) through spatial orbital overlap with the neighboring paramagnetic center, and (ii) an orientation-dependent term, $k_{1\theta}$, arising from the dipolar interaction between the two paramagnets.

In the case of a nonoriented protein in a frozen solution, the relative orientation of the interspin vector and the applied magnetic field is random, and the angle θ between them can take all possible values between 0 and π. The resulting angular distribution of spin−lattice relaxation rates gives rise to non-single-exponential relaxation kinetics. Taking this fact into account, the saturation−recovery EPR transients can be fit by using the following equation:

$$I(t) = 1 - N\int_0^{\pi} \sin\theta \, (e^{-\{k_{1\text{scalar}} + k_{1\theta}\}t}) \, d\theta \qquad (1)$$

where $I(t)$ is the intensity of the saturation−recovery EPR transient at time t, N is an adjustable scaling factor, $k_{1\text{scalar}} = k_{1i} + k_{1ex}$, and $k_{1\theta}$ is expressed by eqs 2 and 3 to follow. Equation 1 is applicable when the anisotropic contribution to the **g** or hyperfine tensor is less than the isotropic contribution, so that the saturation−recovery measurement samples a statistical distribution of orientations, as is the case for the tyrosine radicals (Hirsh et al., 1992).

It has been shown (Hirsh & Brudvig, 1993) that, for the case of a dipolar interaction between an organic radical (slow-relaxing spin) and the non-heme Fe(II) in PSII or in purple bacterial reaction centers (fast-relaxing spin), the C term of the dipolar alphabet is the dominant term in the theoretical expression for $k_{1\theta}$, which is then simplified to the following relation:

$$k_{1\theta} = k_{1d}^{C} \sin^2\theta \cos^2\theta \qquad (2)$$

where

$$k_{1d}^{C} = \frac{3\gamma_s^2\mu_f^2}{r^6}\frac{1}{\omega_s^2 T_{1f}} \qquad (3)$$

In eq 3, r is the interspin distance, γ_s and ω_s are the magnetogyric ratio and the Larmor frequency of the slow-relaxing spin, respectively, and μ_f and T_{1f} are the magnetic moment and the spin−lattice relaxation time of the fast-relaxing spin, respectively. A fit of eq 1 to the experimental saturation−recovery EPR traces extracts two rate constants associated with the observed slow-relaxing spin: $k_{1\text{scalar}}$, which is isotropic and equals the intrinsic relaxation rate in the absence of a significant exchange interaction, and $k_{1\text{dipolar}}$, k_{1d}^{C}, which is expressed in eq 3. As seen in eq 3, the temperature dependence of the dipolar rate constant, k_{1d}^{C}, depends on two terms associated with the fast-relaxing spin (μ_f^2 and T_{1f}). Therefore, the temperature dependence of k_{1d}^{C} provides a signature for the identity of the fast-relaxing spin. The dipolar rate constants measured independently for the $Y_D^{\bullet}$ radical in Mn-depleted PSII and for the bacteriochlorophyll dimer radical, $(BChla)_2^+$, in *Rb. sphaeroides* reaction centers, where the non-heme Fe(II) of the electron-acceptor side is the only other paramagnet, have the same temperature dependence (Hirsh and Brudvig, 1993). On this basis, Hirsh & Brudvig (1993) assigned the non-heme Fe(II) as the relaxation enhancer of $Y_D^{\bullet}$ in Mn-depleted PSII. By using the known distance of 28 Å between $(BChla)_2^+$ and Fe(II) in order to calibrate the observed dipolar rate constants, the $Y_D^{\bullet}$ to non-heme Fe(II) distance was estimated to be 37 ± 5 Å.

In accordance with the dipolar model presented earlier, if the dipole−dipole interaction between the slow- and the fast-relaxing spins is eliminated (as is the case in CN^--treated, Mn-depleted PSII), then the spin−lattice relaxation rate of the observed (slow) spin should decrease significantly and at the same time exhibit single-exponential kinetics. The slow-relaxing spin would then relax with its intrinsic relaxation rate, k_{1i}. In these cases, we have fit the saturation−recovery EPR transients to a single exponential, and the relaxation rate is denoted as $1/T_1$.

The methods used to obtain $1/T_1$, $k_{1\text{scalar}}$, or $k_{1\text{dipolar}}$ have been described previously (Beck et al., 1991; Hirsh et al., 1992). At any given temperature, at least three saturation−recovery EPR transients were recorded at different levels of observing microwave power because the observing microwave power will contribute to the measured isotropic relaxation rate. When a dipolar relaxation mechanism was present, the spin−lattice relaxation was non-single-exponential, and eq 1 was fit to the saturation−recovery EPR transient by using a nonlinear regression program written by Dr. Donald Hirsh, employing the Marquardt algorithm (Press et al., 1989). These fits provided initial values of $k_{1\text{scalar}}$ and $k_{1\text{dipolar}}$. For a noninteracting spin, the spin−lattice relaxation was single-exponential, and an exponential function was used to fit the saturation−recovery transient. These fits provided initial values of $1/T_1$. The true values of $k_{1\text{scalar}}$ and $1/T_1$ were determined by linear extrapolation to zero power. The values of $k_{1\text{dipolar}}$ obtained from the initial fits did not show any dependence on the observing microwave power, and $k_{1\text{dipolar}}$ was taken as the average of values obtained at different levels of observing microwave power.

RESULTS

Spin−Lattice Relaxation of $Y_D^{\bullet}$. Saturation−recovery EPR has been used in the past to probe the spin−lattice relaxation properties of $Y_D^{\bullet}$ in Mn-depleted PSII from spinach (Hirsh et al., 1992; Hirsh & Brudvig, 1993). The saturation−recovery EPR transients showed non-single-exponential kinetics over the entire temperature range employed (5−70 K). A typical saturation−recovery EPR transient obtained for $Y_D^{\bullet}$ (at $T = 9$ K) is shown in Figure 1A (top trace) with the dipolar model fit superimposed. The residuals of single-exponential and dipolar model fits, shown in Figure 1A as the middle and bottom traces, respectively, illustrate the non-single-exponential character of the recovery. The temperature dependence of the dipolar rate constants extracted for $Y_D^{\bullet}$ ($T^{1.6}$) was found to be identical, within experimental error, to that of $(BChla)_2^+$ in *Rb. sphaeroides* reaction centers (Hirsh, 1993). This was taken as strong evidence that, in both cases, the spin−lattice relaxation of the radicals was enhanced by the non-heme Fe(II) of the electron-acceptor side.

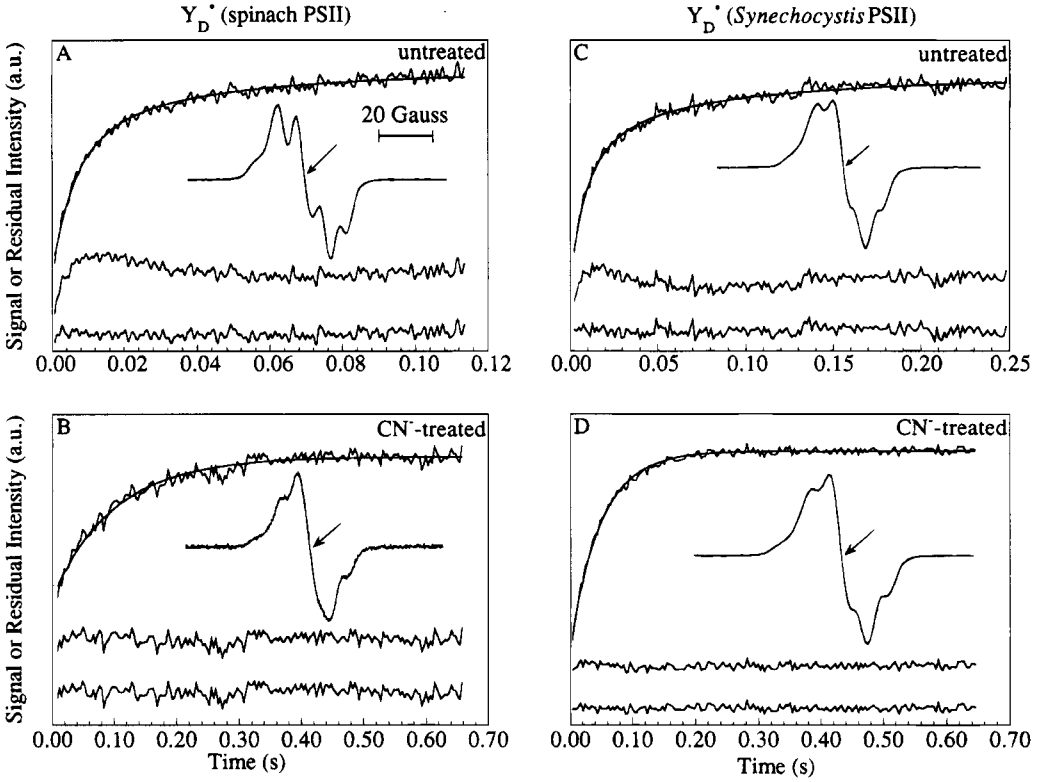

FIGURE 1: Saturation–recovery EPR transients of $Y_D^•$ and residuals (differences between the saturation–recovery transient and fitted curves). The vertical displacements are arbitrary. (A) (Top trace) Saturation–recovery EPR transient of $Y_D^•$ in Mn-depleted spinach PSII at 9.0 K with the dipolar model fit (eqs 1–3) superimposed. The observing microwave power was 1.14 μW, the saturating microwave power was 72 mW, and the pulse was of 20 ms duration [data taken from Hirsh and Brudvig (1993)]. (Middle trace) Residual for a single-exponential fit. (Bottom trace) Residual for the dipolar model fit. (B) (Top trace) Saturation–recovery EPR transient of $Y_D^•$ in CN^--treated (for ~4.5 h), Mn-depleted spinach PSII at 9.1 K with a single-exponential fit superimposed. The observing power was 1.14 μW, the saturating microwave power was 360 mW, and the pulse was of 110 ms duration. (Middle trace) Residual for the single-exponential fit. (Bottom trace) Residual for the dipolar model fit. (C) (Top trace) Saturation–recovery EPR transient obtained for $Y_D^•$ in Mn-depleted, wild-type *Synechocystis* PSII at 10.0 K with the dipolar model fit (eqs 1–3) superimposed. The observing microwave power was 2.28 μW, the saturating microwave power was 144 mW, and the pulse was of 37 ms duration. (Middle trace) Residual for a single-exponential fit. (Bottom trace) Residual for the dipolar model fit. (D) (Top trace) Saturation–recovery EPR transient of $Y_D^•$ in CN^--treated, Mn-depleted, wild-type *Synechocystis* PSII at 10.1 K with a single-exponential fit superimposed. The observing microwave power was 0.29 μW, the saturating microwave power was 360 mW, and the pulse was of 110 ms duration. (Middle trace) Residual for a single-exponential fit. (Bottom trace) Residual for the dipolar-model fit. Insets: cw X-band EPR spectra measured with the following experimental conditions: temperature, 6 K; microwave frequency, 9.07 GHz; field modulation amplitude, 4.0 G; microwave power, 1.44 μW; field modulation frequency, 100 kHz. The arrows indicate the magnetic field setting for the saturation–recovery EPR measurements.

The possibility of selectively converting the non-heme Fe(II) to its low-spin state ($S = 0$) by cyanide treatment (Sanakis et al., 1994) provided us with the means to test this conclusion. The length of dark incubation with CN^- needed to make this conversion complete was decided by following the time course of the yield of the Q_A^- radical EPR signal induced in the dark in a Mn-depleted, CN^--treated, dithionite-reduced PSII sample. Approximately 5 h of incubation with CN^- were needed in order to obtain the maximal yield of ~0.9 spin of Q_A^- per PSII reaction center in spinach PSII samples. Figure 1B (top trace) shows a typical saturation–recovery EPR transient for the $Y_D^•$ radical induced in a Mn-depleted, CN^--treated spinach PSII sample. The recovery is single-exponential, as shown by the superimposed fit and by the identical flat residuals for either the single-exponential fit (Figure 1B, middle trace) or the dipolar model fit (Figure 1B, bottom trace). A comparison of the time scales for the two saturation–recovery EPR traces shown in Figure 1A,B, which were taken at the same temperature, shows that the spin–lattice relaxation of the $Y_D^•$ radical is significantly faster when the non-heme Fe(II) is in its high-spin state ($S = 2$) than when it has been rendered diamagnetic. The saturation–recovery EPR transients of $Y_D^•$ in Mn-depleted, CN^--treated spinach PSII were single-exponential throughout the range of temperatures examined (6–50 K), and the rate constants extracted from single-exponential fits are shown in Figure 3. Their magnitude and temperature dependence ($T^{2.4}$) are very similar to those recently measured (Hirsh et al., 1992) for a model L-tyrosine radical photochemically generated and cryogenically trapped (shown in Figure 3), as well as to the scalar rate constants ($k_{1\text{scalar}}$) extracted from the dipolar model fit in a non-CN^--treated, Mn-depleted sample (Hirsh et al., 1992). These results demonstrate that the spin–lattice relaxation rates measured for $Y_D^•$ in the CN^- derivative of Mn-depleted PSII are the intrinsic relaxation rates of the radical. Overall, the results described earlier confirm that the high-spin form of the non-heme Fe(II) is the fast-relaxing spin that enhances the relaxation of $Y_D^•$ in Mn-depleted spinach PSII. These results also confirm that there is a pairwise dipolar interaction between $Y_D^•$ and the non-heme Fe(II), upon which the dipolar model (eqs 1–3) and the calculation of the distance of 37 ± 5 Å between the two species were based (Hirsh & Brudvig, 1993).

The spin–lattice relaxation of $Y_D^•$ was also studied in Mn-depleted PSII core complexes from *Synechocystis* sp. PCC

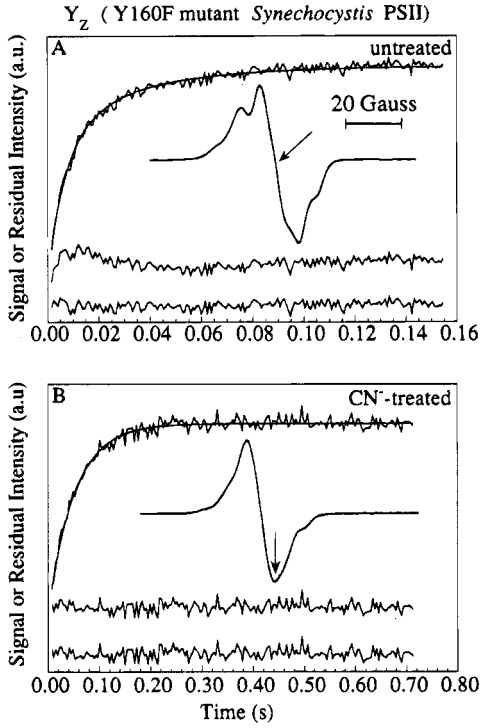

FIGURE 2: Saturation–recovery EPR transients of $Y_Z^\bullet$ and residuals (differences between the saturation–recovery transient and fitted curves). The vertical displacements are arbitrary. (A) (Top trace) Saturation–recovery EPR transient of $Y_Z^\bullet$ in Mn-depleted, Y160F mutant *Synechocystis* PSII at 11.3 K with the dipolar model fit (eqs 1–3) superimposed. The observing microwave power was 3.6 μW, the saturating microwave power was 144 mW, and the pulse was of 23 ms duration. (Middle trace) Residual for a single-exponential fit. (Bottom trace) Residual for the dipolar model fit. (B) (Top trace) Saturation–recovery EPR transient of $Y_Z^\bullet$ in CN^--treated, Mn-depleted Y160F mutant *Synechocystis* PSII at 10.0 K with a single-exponential fit superimposed. The observing microwave power was 0.72 μW, the saturating microwave power was 360 mW, and the pulse was of 120 ms duration. (Middle trace) Residual for a single-exponential fit. (Bottom trace) Residual for the dipolar model fit. Insets: cw X-band EPR spectra measured with the experimental conditions given in Figure 1. The arrows indicate the magnetic field setting for the saturation–recovery EPR measurements.

6803. A typical saturation–recovery EPR transient is shown in Figure 1C (top trace) with the dipolar model fit superimposed. The residuals for single-exponential and dipolar model fits show that the recovery is non-single-exponential. The temperature dependence ($7 < T < 50$ K) of the dipolar rate constants, k_{1d}^C, extracted from the fits is shown in Figure 4. Taking into account the results presented earlier on the spin–lattice relaxation characteristics of the same radical in spinach PSII, we can explain the results from $Y_D^\bullet$ in *Synechocystis* PSII in terms of a pairwise dipolar interaction between $Y_D^\bullet$ and the non-heme Fe(II). In order to test this hypothesis, we measured the spin–lattice relaxation of $Y_D^\bullet$ in the CN^- derivative of *Synechocystis* PSII. A saturation–recovery EPR transient of $Y_D^\bullet$ in CN^--treated *Synechocystis* PSII is shown in Figure 1D (top trace). The recovery shows single-exponential kinetics as seen from the superimposed fit and the residuals. The spin–lattice relaxation rate in the CN^--treated sample is also decreased significantly relative to that observed at the same temperature in a non-CN^--treated sample. The temperature dependence of the spin–lattice relaxation rate in the CN^--treated *Synechocystis* PSII sample ($8 < T < 55$ K) is presented in

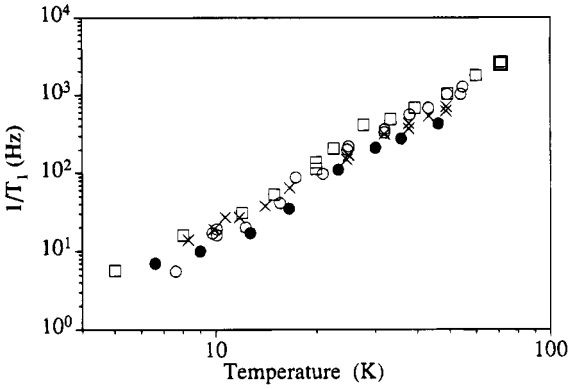

FIGURE 3: Temperature dependence of the intrinsic spin–lattice relaxation rate, $1/T_1$, of the following: model L-tyrosine radical photochemically generated (UV irradiation) and cryogenically trapped [□; data taken from Hirsh et al. (1992)]; $Y_D^\bullet$ in CN^--treated, Mn-depleted spinach PSII (●); $Y_D^\bullet$ in CN^--treated, Mn-depleted wild-type *Synechocystis* PSII (○); $Y_Z^\bullet$ in CN^--treated, Mn-depleted Y160F mutant *Synechocystis* PSII (×). The intrinsic relaxation rates were determined from single-exponential fits to the saturation–recovery EPR traces.

Figure 3 and, within experimental error, it is identical to that of the model tyrosine radical. As in the case of $Y_D^\bullet$ in spinach PSII, we conclude that the non-heme Fe(II) is the only paramagnet acting as a relaxation enhancer of $Y_D^\bullet$ in Mn-depleted PSII isolated from *Synechocystis* sp. PCC 6803.

Spin–Lattice Relaxation of $Y_Z^\bullet$. Due to the use of continuous illumination to induce $Y_Z^\bullet$, some Q_A^- is present in the steady state and is trapped when the sample is frozen. This leads to two considerations. First, it is possible that the relaxation enhancement of $Y_Z^\bullet$ by Q_A^-–Fe(II) is different from that of Q_A–Fe(II). However, we previously showed that the relaxation enhancement of $Y_D^\bullet$ by the non-heme Fe(II) was the same when Q_A was either oxidized or reduced (Koulougliotis et al., 1994). Thus, it is unlikely that the presence of Q_A^- influences the spin–lattice relaxation of $Y_Z^\bullet$. Second, Q_A^- exhibits an EPR signal that overlaps that of $Y_Z^\bullet$ in the CN^--treated sample. The spin–lattice relaxation of Q_A^- has been studied independently (Koulougliotis et al., 1994). In order to assess the contribution of Q_A^- to the saturation–recovery EPR signal of $Y_Z^\bullet$ in the CN^--treated sample, measurements were made as the magnetic field was stepped through the EPR spectrum. (The g values of $Y_Z^\bullet$ and Q_A^- are similar, but the EPR signal from $Y_Z^\bullet$ is broader; therefore, $Y_Z^\bullet$ makes the major contribution to the wings of the EPR spectrum.) At the zero-crossing point, some contribution from Q_A^- was evident in the CN^--treated sample from a non-single-exponential relaxation transient. However, at magnetic fields ≥ 5 G above the magnetic field of the zero-crossing point, the relaxation transients were single-exponential and the value of $1/T_1$ was constant. Therefore, the data in Figures 2 and 3 from the CN^--treated sample were taken at a magnetic field 5 G above the zero-crossing point (indicated by the arrow in the inset to Figure 2B).

$Y_Z^\bullet$ was studied in Mn-depleted PSII core complexes from two different site-directed mutants of *Synechocystis* PSII lacking Y_D (Y160F and Y160M). Saturation–recovery EPR measurements were made on $Y_Z^\bullet$ in both mutants, and the transients showed non-single-exponential kinetics at all temperatures examined ($5 < T < 70$ K). A typical recovery of $Y_Z^\bullet$ in the Y160F mutant is shown in Figure 2A. A single exponential provides a poor fit, while the dipolar model fit

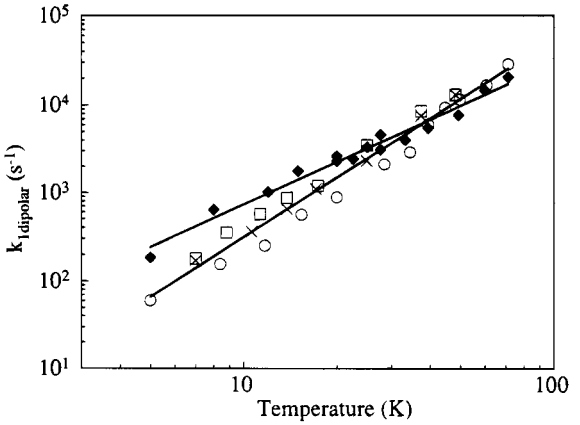

FIGURE 4: Temperature dependence of k_{1d}^C for the following: $Y_D^\bullet$ in Mn-depleted wild-type *Synechocystis* PSII (×); $Y_Z^\bullet$ in Mn-depleted, Y160F mutant *Synechocystis* PSII (□); $Y_Z^\bullet$ in Mn-depleted, Y160M mutant *Synechocystis* PSII (○); $Y_D^\bullet$ in Mn-depleted spinach PSII [◆; data taken from Hirsh and Brudvig (1993)]. The dipolar rate constants were determined from the dipolar model fits (eqs 1−3) to the observed non-single-exponential saturation−recovery EPR traces. The solid lines are least-squares fits to the data: $k_{1d}^C = 1.8T^{2.24}$ ($Y_D^\bullet$ and $Y_Z^\bullet$ in *Synechocystis* PSII) and $k_{1d}^C = 18T^{1.60}$ ($Y_D^\bullet$ in spinach PSII).

is satisfactory. The temperature dependencies of the dipolar rate constants, k_{1d}^C, from the dipolar fits are given in Figure 4 for both the Y160F and Y160M mutants.

The spin−lattice relaxation of $Y_Z^\bullet$ was also examined in the CN^- derivative of Mn-depleted PSII purified from the Y160F mutant. A typical saturation−recovery EPR transient is presented in Figure 2B (top trace). It shows single-exponential kinetics with a significantly decreased rate relative to the non-CN^--treated sample. The magnitude and temperature dependence of the spin−lattice relaxation (Figure 3) are very similar to the corresponding data for a model tyrosine radical and for $Y_D^\bullet$ in Mn-depleted PSII from both spinach and *Synechocystis* (Figure 3). Thus, we conclude that the conversion of the non-heme Fe(II) to its low-spin diamagnetic state eliminates its dipolar interaction with $Y_Z^\bullet$, which consequently relaxes with only its intrinsic spin−lattice relaxation rate.

Locations of Y_D and Y_Z. The experimental results discussed earlier demonstrate that, for both $Y_D^\bullet$ and $Y_Z^\bullet$ in Mn-depleted PSII, the electron acceptor-side non-heme Fe(II) acts as the only source of their observed spin−lattice relaxation enhancement. In this way, the dipolar rate constants (k_{1d}^C) extracted for either radical independently provide a quantitative measure of their distance from the non-heme Fe(II). Figure 4 shows these rate constants for both $Y_D^\bullet$ and $Y_Z^\bullet$ as measured in PSII core complexes from *Synechocystis* sp. PCC 6803. Their identical magnitude and temperature dependence, within experimental error, are direct evidence that $Y_D^\bullet$ and $Y_Z^\bullet$ are located at equal distances from the non-heme Fe(II). Since the $Y_D^\bullet$ to Fe(II) distance has been measured independently (Hirsh & Brudvig, 1993), we conclude that the $Y_Z^\bullet$ to Fe(II) distance also equals 37 ± 5 Å.

DISCUSSION

The spin−lattice relaxation of the dark-stable tyrosine radical in photosystem II, $Y_D^\bullet$, is enhanced by dipole−dipole interactions with other endogenous paramagnetic centers. Previously, the non-heme Fe(II) was assigned as the relaxation enhancer of $Y_D^\bullet$ in Mn-depleted PSII, on the basis of the identical temperature dependencies of the dipolar relaxation rates of $Y_D^\bullet$ in Mn-depleted spinach PSII and of $(BChla)_2^+$ in the reaction center from *Rb. sphaeroides* (Hirsh & Brudvig, 1993). The results of saturation−recovery EPR measurements on $Y_D^\bullet$ in CN^--treated, Mn-depleted PSII (Figure 1) definitively show that the non-heme Fe(II) is the sole relaxation enhancer of $Y_D^\bullet$ in both spinach and *Synechocystis* PSII. The non-heme Fe(II) was also identified as the relaxation enhancer of $Y_Z^\bullet$ in *Synechocystis* PSII (Figure 2).

As shown in eq 3, the temperature dependence of $k_{1dipolar}$ is determined by the magnetic properties of the fast-relaxing spin. In the cases of $Y_D^\bullet$ in Mn-depleted spinach PSII, $Y_D^\bullet$ and $Y_Z^\bullet$ in Mn-depleted *Synechocystis* PSII, and $(BChla)_2^+$ in the reaction center from *Rb. sphaeroides*, the homologous non-heme Fe(II) is the fast-relaxing spin. A comparison of the temperature dependence of $k_{1dipolar}$ of these four radicals, therefore, provides a comparison of the magnetic properties of the non-heme Fe(II) in the different proteins. In *Synechocystis* PSII, the temperature dependence of k_{1d}^C is identical for both $Y_D^\bullet$ and $Y_Z^\bullet$ ($T^{2.24}$, Figure 4). On the other hand, it is slightly different from those observed for $Y_D^\bullet$ in Mn-depleted spinach PSII ($T^{1.60}$, Figure 4) or $(BChla)_2^+$ in *Rb. sphaeroides* reaction centers [data not shown, see Hirsh and Brudvig (1993)]. In the latter two cases, the temperature dependence of k_{1d}^C is identical (Hirsh & Brudvig, 1993). These results indicate that the magnetic properties of the non-heme Fe(II) in spinach PSII and in *Rb. sphaeroides* reaction centers are quite similar, but that the magnetic characteristics (e.g., g factor or zero-field splittings) of the non-heme Fe(II) in *Synechocystis* PSII may be slightly different.

Another difference between spinach and *Synechocystis* PSII is the time needed for quantitative conversion of the non-heme Fe(II) to its low-spin diamagnetic state by CN^- treatment: ~5 h for PSII isolated from spinach compared to ~0.5 h for PSII isolated from *Synechocystis* sp. PCC 6803. This difference in chemical reactivity may reflect the slightly different coordination environments of the non-heme Fe(II) in spinach and in *Synechocystis* PSII, or it may be due to the spinach PSII being a membrane preparation while the *Synechocystis* PSII is a core complex.

On the other hand, the magnitude and temperature dependence of the intrinsic spin−lattice relaxation of $Y_D^\bullet$ are very similar in both spinach and *Synechocystis* PSII (Figure 3), even though, according to Rigby et al. (1994) and Warncke et al. (1994), the β-proton hyperfine coupling constants are slightly different for $Y_D^\bullet$ in the two species. Our results indicate that these variations in the electronic structure of $Y_D^\bullet$ do not have a measurable effect on its intrinsic spin−lattice relaxation rate. As seen in Figure 3, $Y_Z^\bullet$ and $Y_D^\bullet$ have identical intrinsic spin−lattice relaxation rates, which are also very similar to the ones recently observed for the tyrosine radical in the R2 subunit of ribonucleotide reductase (R2-RNR) isolated from *Salmonella thyphimurium* (Galli et al., 1995). In that study, it was shown that the spin−lattice relaxation rate of *Salmonella* R2-RNR was considerably slower than those of the tyrosine radicals in R2-RNR enzymes isolated from mouse, herpes simplex virus 1, or *Escherichia coli*. The uniqueness of the tyrosine radical in the *Salmonella* R2-RNR protein is the magnitude of the β-proton hyperfine interaction: it is similar

to that of either $Y_D^•$ or $Y_Z^•$ and considerably smaller than that of either the mouse, herpes simplex virus 1, or *E. coli* R2-RNR tyrosine radical. Thus, the observation of identical and considerably slower intrinsic spin−lattice relaxation rate constants for the $Y_D^•$, $Y_Z^•$, and *Salmonella* R2-RNR tyrosine radicals is in accordance with the conclusion of Galli et al. (1995) that the dominant contribution to the intrinsic spin−lattice relaxation rate of the tyrosine radicals is the modulation of the β-proton hyperfine interaction by thermal lattice motions.

CONCLUSION

In this paper, we present direct experimental evidence for a pairwise dipolar interaction between either $Y_D^•$ or $Y_Z^•$ and the electron-acceptor side non-heme Fe(II) in Mn-depleted PSII. This dipolar interaction causes spin−lattice relaxation enhancement, as well as non-single-exponential relaxation kinetics, of both tyrosine radicals. Because the magnitude of this dipolar interaction is identical for both $Y_D^•$ and $Y_Z^•$, we conclude that they are located at equal distances from the non-heme Fe(II). On the basis of the results of Hirsh and Brudvig (1993), in which the known $(BChla)_2^+$−Fe(II) distance was used for calibration, the distances in PSII are estimated to be $r_{Y_D^•-Fe(II)} = r_{Y_Z^•-Fe(II)} = 37 \pm 5$ Å. These results provide the first spectroscopic evidence for a symmetric location of tyrosines D and Z in PSII and are consistent with the existence of a C_2 symmetry axis among the chromophores of PSII, as in the purple bacterial reaction center.

REFERENCES

Abragam, A. (1955) *Phys. Rev. 98*, 1729−1735.

Abragam, A. (1961) *The Principles of Nuclear Magnetism*, Clarendon Press, Oxford, UK.

Allen, J. P., Feher, G., Yeates, T. O., Komiya, H., & Rees, D. C. (1988) *Proc. Natl. Acad. Sci. U.S.A. 85*, 8487−8491.

Barry, A. B., & Babcock, G. T. (1987) *Proc. Natl. Acad. Sci. U.S.A. 84*, 7099−7103.

Barry, B. A., & Babcock, G. T. (1988) *Chem. Scr. 28A*, 117−122.

Beck, W. F., de Paula, J. C., & Brudvig, G. W. (1985) *Biochemistry 24*, 3035−3043.

Beck, W. F., Innes, J. B., & Brudvig, G. W. (1990) in *Current Research in Photosynthesis* (Baltscheffsky, M., Ed.) pp 817−820, Kluwer Academic Publishers, Dordrecht, The Netherlands.

Beck, W. F., Innes, J. B., Lynch, J. B., & Brudvig, G. W. (1991) *J. Magn. Reson. 91*, 12−29.

Berthold, D. A., Babcock, G. T., & Yocum, C. F. (1981) *FEBS Lett. 134*, 231−234.

Bloembergen, N. (1949) *Physica 15*, 386−426.

Boerner, R. J., & Barry, B. A. (1993) *J. Biol. Chem. 268*, 17151−17154.

Bowyer, J., Hilton, M., Whitelegge, J., Jewess, P., Camilleri, P., Crofts, A., & Robinson, H. (1990) *Z. Naturforsch. 45c*, 379−387.

Buser, C. A., Thompson, L. K., Diner, B. A., & Brudvig, G. W. (1990) *Biochemistry 29*, 8977−8985.

Chang, C. H., Tiede, D., Tang, J., Smith, U., Norris, J., & Schiffer, M. (1986) *FEBS Lett. 205*, 82−86.

Debus, R. J., Barry, B. A., Babcock, G. T., & McIntosh, L. (1988a) *Proc. Natl. Acad. Sci. U.S.A. 85*, 427−430.

Debus, R. J., Barry, B. A., Sithole, I., Babcock, G. T., & McIntosh, L. (1988b) *Biochemistry 27*, 9071−9074.

Deisenhofer, J., Epp, O., Miki, K., Huber, R., & Michel, H. (1985) *Nature 318*, 618−624.

Evelo, R. G., Styring, S., Rutherford, A. W., & Hoff, A. J. (1989) *Biochim. Biophys. Acta 973*, 428−442.

Galli, C., Atta, A., Andersson, K. K., Gräslund, A., & Brudvig, G. W. (1995) *J. Am. Chem. Soc. 117*, 740−746.

Hirsh, D. J. (1993) Ph.D. Thesis, Yale University, New Haven, CT.

Hirsh, D. J., & Brudvig, G. W. (1993) *J. Phys. Chem. 97*, 13216−13222.

Hirsh, D. J., Beck, W. F., Innes, J. B., & Brudvig, G. W. (1992) *Biochemistry 31*, 532−541.

Hoganson, C. W., & Babcock, G. T. (1988) *Biochemistry 27*, 5848−5855.

Hyde, J. S. (1979) in *Time-Domain Electron Spin Resonance* (Kevan, L., & Schwartz, R. N., Eds.) pp 1−30, John Wiley & Sons, New York.

Ikeuchi, M., & Inoue, Y. (1987) *FEBS Lett. 210*, 71−76.

Kirmaier, C., &Holten, D. (1987) *Photosynth. Res. 13*, 225−260.

Koulougliotis, D., Innes, J. B., & Brudvig, G. W. (1994) *Biochemistry 33*, 11814−11822.

Metz, J. G., Nixon, P. J., Rögner, M., Brudvig, G. W., & Diner, B. A. (1989) *Biochemistry 28*, 6960−6969.

Michel, H., & Deisenhofer, J. (1988) *Biochemistry 27*, 1−7.

Michel, H., Weyer, K. A., Gruenberg, H., Dunger, I., Oesterhelt, D., & Lottspeich, F. (1986) *EMBO J. 5*, 1149−1158.

Press, W. H., Flannery, B. P., Teukolsky, S. A., & Vetterling, W. T. (1989) *Numerical Recipes in Pascal*, Cambridge University Press, Cambridge, UK.

Rigby, S. E. J., Nugent, J. H. A., & O'Malley, P. J. (1994) *Biochemistry 33*, 1734−1742.

Rögner, M., Nixon, P. J., & Diner, B. A. (1990) *J. Biol. Chem. 265*, 6189−6196.

Ruffle, S. V., Donnelly, D., Blundell, T. L., & Nugent, J. H. A. (1992) *Photosynth. Res. 34*, 287−300.

Sanakis, Y., Petrouleas, V., & Diner, B. A. (1994) *Biochemistry 33*, 9922−9928.

Sayre, R. T., Andersson, B., & Bogorad, L. (1986) *Cell 47*, 601−608.

Styring, S., & Rutherford, A. W. (1988) *Biochemistry 27*, 4915−4923.

Svensson, B., Vass, I., Cedergren, E., & Styring, S. (1990) *EMBO J. 9*, 2051−2059.

Takahashi, Y., Satoh, K., & Takahashi, M. (1986) *FEBS Lett. 208*, 347−351.

Tang, X.-S., & Diner, B. A. (1994) *Biochemistry 33*, 4594−4603.

Tang, X.-S., Zheng, M., Chisholm, D. A., Dismukes, G. C., & Diner, B. A. (1995) *Biochemistry* (submitted for publication).

Thompson, L. K., & Brudvig, G. W. (1988) *Biochemistry 27*, 6653−6658.

Tietjen, K. G., Kluth, J. F., Andree, R., Haug, M., Lindig, M., Müller, K. H., Wroblowsky, H. J., & Trebst, A. (1991) *Pestic. Sci. 31*, 65−72.

Trebst, A. (1986) *Z. Naturforsch. 41c*, 240−245.

Vermaas, W. F. J., Rutherford, A. W., & Hansson, Ö. (1988) *Proc. Natl. Acad. Sci. U.S.A. 85*, 8477−8481.

Warncke, K., Babcock, G. T., & McCracken, J. (1994) *J. Am. Chem. Soc. 116*, 7332−7340.

BI942234Z